

RSC Advances



This is an *Accepted Manuscript*, which has been through the Royal Society of Chemistry peer review process and has been accepted for publication.

Accepted Manuscripts are published online shortly after acceptance, before technical editing, formatting and proof reading. Using this free service, authors can make their results available to the community, in citable form, before we publish the edited article. This *Accepted Manuscript* will be replaced by the edited, formatted and paginated article as soon as this is available.

You can find more information about *Accepted Manuscripts* in the [Information for Authors](#).

Please note that technical editing may introduce minor changes to the text and/or graphics, which may alter content. The journal's standard [Terms & Conditions](#) and the [Ethical guidelines](#) still apply. In no event shall the Royal Society of Chemistry be held responsible for any errors or omissions in this *Accepted Manuscript* or any consequences arising from the use of any information it contains.



Synthesis of Mo-doped TiO₂ Nanowires/Reduced Graphene Oxide Composites with Enhanced Photodegradation Performance under Visible Light Irradiation†

Shanshan Zhu,^a Yuming Dong,^a Xiaofeng Xia,^a Xiang Liu^{*a} and Hexing Li^{*b}

In this research, anatase type Mo-doped TiO₂ nanowires/reduced graphene oxide (Mo-TiO₂NWs/RGO) composites were successfully synthesized using a one-step alkali hydrothermal method followed by a calcination treatment at 500°C, in which commercial TiO₂ nanoparticles (Degussa P25) and graphene oxide (GO) were used as the precursors. GO was reduced to RGO during the alkali hydrothermal progress, and Mo was incorporated into the lattice of TiO₂ nanowires (TiO₂NWs) simultaneously. The samples were characterized by X-ray diffraction (XRD), Raman spectroscopy, thermogravimetric analysis (TGA), Fourier-transform infrared spectroscopy (FTIR), X-photoelectron spectroscopy (XPS), inductively coupled plasma-atomic emission spectrometry (ICP-AES), scanning electron microscope (SEM), transmission electron microscope (TEM) and UV-visible diffuse reflectance spectroscopy (DRS). The photocatalytic properties of the prepared catalysts were evaluated for the photodegradation of methylene blue (MB) under visible light irradiation. The results showed that Mo-TiO₂NWs/RGO composites exhibited much higher photocatalytic activity in comparison to the mono-modified or non-modified TiO₂NWs, the photodegradation efficiency of Mo-TiO₂NWs/RGO composites could reach up to 94.1% in 120 min, and no obvious deactivation was observed in the durability experiments. The mechanism of the enhanced photocatalytic activity, which aroused from the synergistic effect of morphology modification, Mo doping and graphene incorporation, was put forward.

Received 00th January 20xx,
Accepted 00th January 20xx

DOI: 10.1039/x0xx00000x

www.rsc.org/

1. Introduction

Since the pioneering discovery of photocatalytic activity in early 1970s¹, TiO₂ has attracted extensive attention in catalytic field during the past decades due to the promising potentials such as inexpensive cost, high chemical stability and environment friendly². Nevertheless the relatively wide band gap and rapid recombination of the photoexcited electron-hole pairs result in the lack of visible light absorption ($\lambda < 380$ nm) and the loss of practically 90% of the excited carriers³. Therefore, plenty of strategies have been developed to modify intrinsic TiO₂ aiming at extending light-response range to the visible region and prolonging lifetime of the photogenerated electron-hole pairs, including doping^{4, 5}, loading with noble metal⁶, constructing unique geometry⁷, coupling with other semiconductor⁸, metal oxides^{9, 10} and carbonaceous materials¹¹⁻¹⁶. Compared to other carbonaceous materials, graphene has gotten extraordinary attention to fabricate novel TiO₂-graphene composite photocatalysts as a consequence of its distinct two-

dimensional (2D) morphology and extraordinary optical, mechanical, thermal, and electrical attributes¹⁷⁻¹⁹. The combination of graphene and TiO₂ can tremendously improve the photocatalytic performance due to the enhance adsorption of pollutants, extended light absorption range and enhanced charge separation and transportation^{18, 20, 21}.

Nevertheless, limited visible light absorption and rapid recombination of photogenerated electron-hole pairs are still the primary obstacles to use solid photocatalysts in aqueous medium. The photocatalytic activity of TiO₂-graphene composites can be further strengthen either by facilitating the visible light absorption or by restraining the recombination of photo-excited electron-hole pairs through the incorporation of other species to the composites. For instance, Nguyen-Phan and co-workers²² reported a hydrothermal method for the preparation of Sn-doped TiO₂ nanoparticles supported onto reduced graphene oxide (RGO), which showed excellent photocatalytic performance. Qian et al.²³ prepared N-doped TiO₂/graphene composites which showed superior photocatalytic efficiency due to the synergistic roles of the conductive carbon platform and the N-doped TiO₂. Zhang et al.²⁴ synthesized the visible-light responsive magnetic Fe₂O₃/TiO₂/graphene hybrid photocatalysts and the photodegradation results showed that the hybrids possessed impressive visible-light photocatalytic performance than other samples.

Despite the above-mentioned promising results, there are still some defects since TiO₂ nanoparticles turn to

^aThe Laboratory of Food Colloids and Biotechnology, Ministry of Education, School of Chemical and Material Engineering, Jiangnan University, Wuxi 214122, P. R. China. E-mail: liuxiang@jiangnan.edu.cn

^bThe Key Laboratory of the Chinese Ministry of Education in Resource Chemistry, Shanghai Normal University, Shanghai 200234, P. R. China. E-mail: hexing-li@shnu.edu.cn

† Electronic Supplementary Information (ESI) available. See DOI: 10.1039/x0xx00000x

agglomerate on RGO, which would prohibit the direct chemical contact between these two components, and thus may immensely weaken the synergetic catalytic effect of RGO and TiO₂ nanoparticles²⁵. Thus, if we use appropriate methods to modify TiO₂ morphology, such as constructing one-dimensional (1D) structured TiO₂ nanowires, this problem will be avoided. In our previous study, we had prepared graphene/Fe³⁺-doped TiO₂ nanowire composites (GR/Fe-NWCs) through a facile hydrothermal method, and the photocatalytic performance of GR/Fe-NWCs for methylene blue (MB) under visible light was much higher than other photocatalysts²⁶. In addition, many theoretical and experimental studies had demonstrated that Mo-doped TiO₂ materials presented enhanced photocatalytic activity and photoelectrochemical performance compared with pristine TiO₂²⁷⁻³⁰.

Therefore, if we can employ more strategies together to modify TiO₂, for example, doping with metal or nonmetal element into the pristine TiO₂, constructing 1D structured TiO₂ and incorporating with graphene, the photocatalytic activity of the finally synthesized photocatalysts may be further enhanced. Herein, we prepared Mo-doped TiO₂ nanowires/reduced graphene oxide (Mo-TiO₂NWs/RGO) composites for the first time via a facile alkali hydrothermal method followed by a calcination treatment and investigated their photocatalytic activity towards the photodegradation of MB, a representative dye, under visible light irradiation. The photodegradation results demonstrated that Mo-TiO₂NWs/RGO composites exhibited remarkable improvement for decomposing MB when compared with the mono-modified TiO₂NWs and non-modified TiO₂NWs. Moreover, the mechanism we put forward could explain the synergistic effect of these modification methods.

2. Experimental section

2.1 Materials

Commercial TiO₂ nanoparticles (Degussa P25) were purchased from Evonik-Degussa. Graphite flakes (Aldrich), Methylene Blue (MB) and other chemicals were obtained from Sinopharm Chemical Reagent Company. All reagents were of analytical grade without any further purification.

2.2 Synthesis of Graphene Oxide (GO)

GO was prepared from natural graphite flakes applying a modified Hummer's method³¹, the specific procedure was described previously²⁶.

2.3 Synthesis of Mo-doped TiO₂ nanowires/reduced graphene oxide (Mo-TiO₂NWs/RGO) composites

Mo-TiO₂NWs/RGO composites were synthesized using a modified alkali hydrothermal process³² followed a calcination treatment. In a typical preparation route, firstly, 50 mg of as-prepared GO was put into 60 ml of deionized water and underwent sonication for 2 h. Next, 1.0g commercial TiO₂ nanoparticles (Degussa P25) and 0.011g (NH₄)₆Mo₇O₂₄·4H₂O

(containing 0.5 at% of Mo) were added to the GO suspension and stirred another 30min to obtain a homogeneous greyish suspension. After the addition of 40g of KOH, the suspension was transferred into a Teflon-sealed autoclave of 100 mL capacity and kept at 200°C for 24 h. After being cooled down to room temperature, the resulting gel was washed with 0.1M HCl aqueous solution, deionized water and ethanol for several times until the resulting pH was neutral. After being recovered by centrifugation, the wet product was dried at 60°C and annealed at 500°C for 2 h under N₂ atmosphere. For comparison, TiO₂ nanowires/reduced graphene oxide (denoted as TiO₂NWs/RGO) composites, Mo-doped TiO₂ nanowires (Mo-TiO₂NWs) and TiO₂ nanowires (TiO₂NWs) were also synthesized using the same hydrothermal method except addition of Mo or/and GO sources. In addition, Mo-TiO₂NWs as well as TiO₂NWs were annealed in the air.

Furthermore, in order to investigate the influence of RGO content on the photocatalytic activity of Mo-TiO₂NWs/RGO composites, the proportions of GO to Mo-TiO₂NWs were designed by varying the added amount of GO (10, 50, 100 and 200 mg), and the obtained samples were marked as Mo-TiO₂NWs/RGO-x, where x = 1, 5, 10 and 20, respectively. After the photocatalytic research of the series of Mo-TiO₂NWs/RGO-x composites, Mo-TiO₂NWs/RGO-5 composites show the best photocatalytic activity compared with others (Fig. S1, ESI[†]), so the Mo-TiO₂NWs/RGO-5 composites were used as the followed Mo-TiO₂NWs/RGO composites.

2.4. Characterizations

Powder X-ray diffraction (XRD) patterns of the samples were performed by Bruker D8 Advance diffractometer (Bruker AXS Ltd., Germany) using Cu K α radiation, operated at 40 kV and 30 mA in the range of 5–80° (2 θ). Scanning electron microscopy (SEM) was collected with an S-4800 scanning electron analyzer (Hitachi, Ltd., Japan) with an accelerating voltage of 15 Kv. The transmission electron microscopy (TEM) images were carried out by JEM-2100 instrument (JEOL, Japan) operating at an accelerating voltage of 200 kV. Raman spectra measurements were recorded with an inVia Reflex Raman spectrometer (Renishaw Ltd., United Kingdom) with 532 nm laser excitation. Thermogravimetric analysis (TGA) was performed on a TGA/1100SF thermoanalyzer (Mettler Toledo, Switzerland) in air flow at a heating rate of 10°C/min. Fourier Transform Infrared (FTIR) spectra were acquired on a Nicolet iS50 FT-IR spectrophotometer (Thermo Fisher Scientific Inc., USA) in the range of 4000-400cm⁻¹ with KBr as the reference sample. UV-vis diffuse reflectance spectra (DRS) were measured using a UV-2550 spectrometer (Shimadzu, Japan) in the wavelength region from 200 to 800 nm, in which BaSO₄ was used as the background. The surface electronic states were analyzed by Versa Probe PHI 5000 XPS (Ulvac-PHI, INC. Japan). All the binding energy (BE) values were calibrated based on the containment carbon (C1s 284.6 eV). The real atom content of Mo in the as-prepared samples

was conducted on ICP-AES (VISTA-MPXICP-OES, Varian Ltd, USA).

2.5 Evaluation of photocatalytic activity and endurance

The photocatalytic activities of the prepared photocatalysts were evaluated by measuring the photodecomposition of methylene blue (MB) aqueous solution under visible light irradiation using a 400W Xe lamp with a UV-CUT filter ($\lambda > 380$ nm) as the light source, and the distance between the lamp and the solutions was about 15 cm. In a representative procedure, 60 mg of photocatalysts were dispersed in 500mL of 10 mg/L MB aqueous solution. Before irradiation, the suspension was magnetically stirred in the dark for 1h in order to establish an adsorption/desorption equilibrium between the photocatalysts and MB. At given time intervals, about 5mL photoreacted solution was collected and then centrifuged to remove any suspended solid photocatalysts. The initial and remaining concentration of MB was calculated via analyzing the absorbance measured on a UV-vis spectrophotometer at the wavelength of 663 nm since the concentration changes (C/C_0) of MB were proportional to the absorbance (A/A_0) during the photodegradation, where C_0 and A_0 are the initial concentration and absorbance of MB, respectively, C and A refer to the concentration and absorbance of MB at real time t , respectively. As a contrast, a control sample composed of P25+RGO by physical blending and a blank test without photocatalysts were implemented as well.

What's more, five successive cycles were tested to examine the durability and reusability of the Mo-TiO₂NWs/RGO photocatalysts toward the degradation of MB under visible light irradiation, each lasting for 120 min. After each cycle, the photocatalysts were filtered and washed thoroughly with deionized water and ethanol, and then dried at 60°C for the next experiment.

3. Results and discussion

3.1 Sample characterization

XRD was used to analyze the crystalline phases of different samples as illustrated in Fig. 1. It can be seen that TiO₂NWs, Mo-TiO₂NWs, TiO₂NWs/RGO and Mo-TiO₂NWs/RGO composites (Fig. 1 (a)-(d)) have similar diffraction peaks at $2\theta = 25.3^\circ, 37.8^\circ, 48.0^\circ, 53.9^\circ, 55.1^\circ, 62.7^\circ, 68.8^\circ, 70.3^\circ$ and 75.0° corresponding to (101), (004), (200), (105), (211), (204), (116), (220) and (215) planes of the anatase TiO₂ (JCPDS No.21-1272), respectively. And no obvious characteristic peaks of MoO₃ are detected in Mo-TiO₂NWs and Mo-TiO₂NWs/RGO composites, which could be explained by the low dopant amount or even dispersion of MoO₃³³. In addition, it should be noted that GO (Fig. 1(e)) has a diffraction peak at $2\theta = 10.25^\circ$ corresponding to (002) peak with an interlayer distance of 10.9Å, indicating that the pristine graphite was oxidized into GO with a highly-ordered layered structure³⁴. Compared with the GO, this characteristic peak in TiO₂NWs/RGO and Mo-TiO₂NWs/RGO composites

disappear after the alkali hydrothermal process demonstrating that most of GO was successfully reduced to graphene. The typical peak of graphene at about $2\theta = 25^\circ$ can't be detected, which can be attributed to the insufficient amount and relatively weak diffraction intensity of graphene in the composites³⁴⁻³⁶.

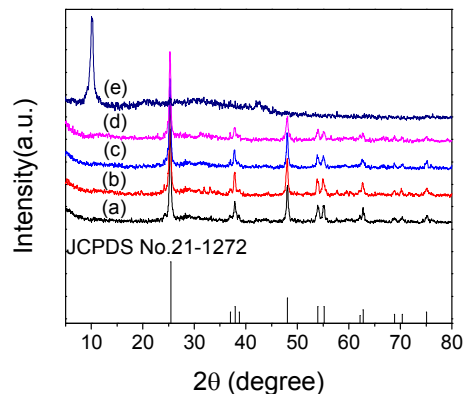


Fig. 1. XRD patterns of TiO₂NWs (a), Mo-TiO₂NWs (b), TiO₂NWs/RGO (c), Mo-TiO₂NWs/RGO (d) and GO (e).

Raman spectroscopy is one of the most powerful tools to detect the structural and electronic properties of graphene-based materials. As observed in Fig. 2(a)-(d), four remarkable peaks observed in the low frequency region are assigned to the $E_{1g(1)}$ (145 cm^{-1}), $B_{1g(1)}$ (399 cm^{-1}), $A_{1g}+B_{1g(2)}$ (516 cm^{-1}) and $E_{g(2)}$ (637 cm^{-1}) modes of anatase phase of TiO₂, respectively³⁷. In the Raman spectrum of GO (Fig. 2(e)), the D and G bands can be observed at around 1342 cm^{-1} and 1586 cm^{-1} , respectively. It is well-known that D band is a general character of sp^3 defects in carbon and G band exhibits information on in-plane vibrations of sp^2 bonded carbons^{32, 38, 39}. While compared with GO, the G band of TiO₂NWs/RGO and Mo-TiO₂NWs/RGO composites shifts to 1603 cm^{-1} after the hydrothermal process. The blueshift of the G band can be ascribed to the transformation of graphite to graphene sheets or the resonant vibration of isolated double bonds in higher frequencies³². In addition, the calculated I_D/I_G intensity ratio is 1.25 for GO and 1.13 for both TiO₂NWs/RGO and Mo-TiO₂NWs/RGO composites. The decrease of I_D/I_G intensity ratio indicates the remove of hydroxyl and epoxy groups and the restoration of sp^2 -bonded carbons, affirming the presence of graphene sheets in the TiO₂NWs/RGO and Mo-TiO₂NWs/RGO composites¹⁹. And the TGA analysis (Fig. S2, ESI†) shows that the amount of RGO in Mo-TiO₂NWs/RGO composites is about 5.07 wt%. These results are consistent with the XRD studies.

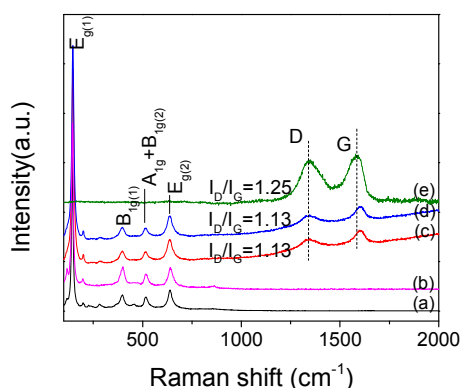


Fig. 2. Raman spectra of TiO₂NWs (a), Mo-TiO₂NWs (b), TiO₂NWs/RGO (c), Mo-TiO₂NWs/RGO (d) and GO (e).

FTIR spectra were measured to further prove the reduction of GO after hydrothermal treatment. The broad peaks at around 3400 cm⁻¹ and 1390 cm⁻¹ for GO and Mo-TiO₂NWs/RGO composites (Fig. S3, ESI[†]) are attributed to the surface O-H and tertiary C-OH, respectively³. In addition, the absorption peak at about 1600 cm⁻¹ is assigned to the skeletal vibration of graphene^{35, 37}. The spectrum of GO (Fig. S3(a), ESI[†]) displays characteristic peaks of oxygen-containing functional groups such as carboxyl C=O (1723 cm⁻¹), epoxy C-O (1271 cm⁻¹), alkoxy C-O (1043 cm⁻¹), which verified that the graphite was successfully oxidized to GO. Whereas, for the Mo-TiO₂NWs/RGO composites (Fig. S3(b), ESI[†]), the intensities of these oxygen-containing functional groups decrease sharply, confirming a significant reduction of GO through the hydrothermal reaction. Moreover, the broad absorbance band at low frequency (below 1000 cm⁻¹) is allocated to the stretching vibration of Ti-O-Ti bonds^{19, 34, 40}. And the band at about 467 cm⁻¹ was consistent with Ti-O stretching of the anatase TiO₂⁴¹.

In order to analyze the different chemical conditions of Mo-TiO₂NWs/RGO composites as well as the existence of Mo and the interactions between TiO₂ and graphene in the compounds, the samples were characterized by XPS. Fig. 3(a) reveals the XPS survey spectrum of GO, which exhibits obvious C 1s and O 1s peaks at 284.6 eV and 532.5 eV, respectively. While compared with GO, the XPS survey spectrum of Mo-TiO₂NWs/RGO composites (Fig. 3(b)) indicates the existences of elements Ti and Mo in the composites. As can be seen from the inset in Fig. 3(b), two prominent peaks were recorded at the binding energies of 458.5 eV and 464.2 eV, corresponding to Ti 2p_{3/2} and Ti 2p_{1/2} signals in the Ti⁴⁺ chemical form, respectively^{19, 42}. Fig. 3(c) presents the high-resolution XPS spectrum of Mo 3d region, the binding energies of 232.2 eV and 235.3 eV can be attributed to the feature of Mo⁶⁺, while 231.2 eV and 234.3 eV correspond to the presence of Mo⁵⁺ in the lattice of TiO₂NWs³⁰. Thereby, we can draw the conclusion that Mo was doped into the lattice of TiO₂NWs and coexisted in the forms of Mo⁶⁺ and Mo⁵⁺ in Mo-TiO₂NWs/RGO composites. Furthermore, according to the ICP-AES, the real atom content of Mo in the Mo-TiO₂NWs/RGO composites is 0.42 at.%. The

high-resolution C1s XPS spectra for GO and Mo-TiO₂NWs/RGO composites are illustrated in Fig. 3(d) and 3(e), respectively. For GO (Fig. 3(d)), the peak centered at 284.6 eV is corresponded to the C-C, C=C and C-H bonds¹⁹, and the other peaks at 286.7 eV and 287.8 eV are assigned to C-O in hydroxyl or epoxy groups and C=O³⁴, respectively. Nonetheless, the peak intensities of these oxygen-containing functional groups dramatically reduced in the C 1s XPS spectrum of Mo-TiO₂NWs/RGO composites (Fig. 3(e)), revealing that GO was mostly reduced to RGO. Furthermore, the O1s XPS spectrum of GO is located at 532.5 eV, which is closely related to the abundant hydroxyl groups on the surface of GO¹⁹, while this peak shifts to 529.7 eV for Mo-TiO₂NWs/RGO composites, as shown in Fig. 3(f). This chemical shift may be assigned to the formation of Ti-O-C bond in the composites¹⁹. These mentioned results indicate that Mo was successfully incorporated into the lattice of TiO₂NWs, further demonstrate the effective reduction of GO and the existence of the integration between TiO₂NWs and graphene in the composites after the hydrothermal treatment.

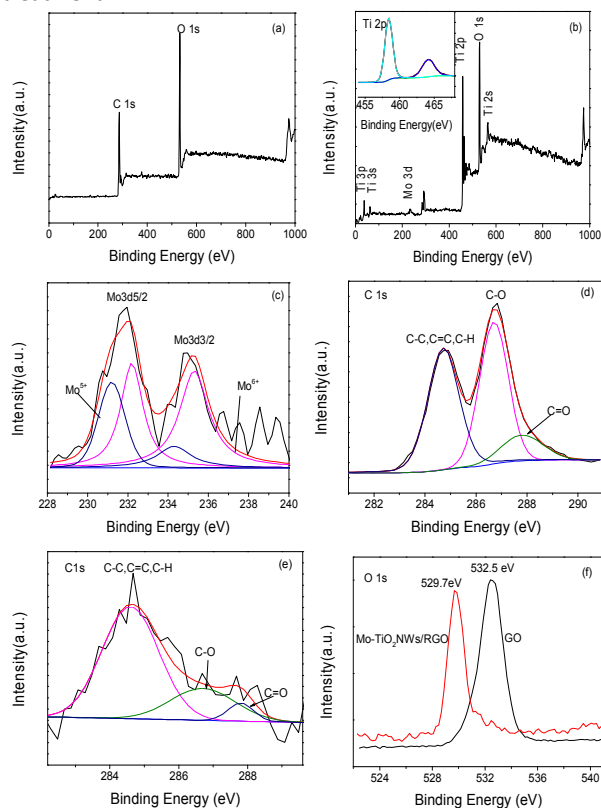


Fig. 3. Full XPS spectra of GO (a) and Mo-TiO₂NWs/RGO (b); fitted XPS spectra of Mo of Mo-TiO₂NWs/RGO (c); fitted C1s XPS of GO (d) and Mo-TiO₂NWs/RGO (e); O 1s XPS spectra of GO and Mo-TiO₂NWs/RGO (f).

The micro-morphologies of the as-obtained Mo-TiO₂NWs/RGO composites were characterized by SEM and TEM, as displayed in Fig. 4. As can be seen from SEM images (Fig. 4(a)-(b)) that plenty of 1D nanostructured Mo-TiO₂NWs

are dispersed on the surface of RGO after hydrothermal treatment with an average diameter of about 10nm and length of several hundred nanometers. Nevertheless, the graphene nanosheets in the composites are not obvious due to their low contrast in SEM. Hence, TEM was used to further illustrate the structure of Mo-TiO₂NWs/RGO composites. The typical TEM images (Fig. 4(c)-(d)) reveals that the RGO is layered morphology with smooth surface, playing the role of a matrix for the concentrated Mo-TiO₂NWs. It is effortless to observe that the Mo-TiO₂NWs immensely take up the utilizable surface area of RGO, resulting much abundant attachment of Mo-TiO₂NWs in the composites. Obviously, this reasonably uniform nanostructure can guarantee direct chemical contact between Mo-TiO₂NWs and graphene, thus improving the efficiency of photodegradation for organic pollutants.

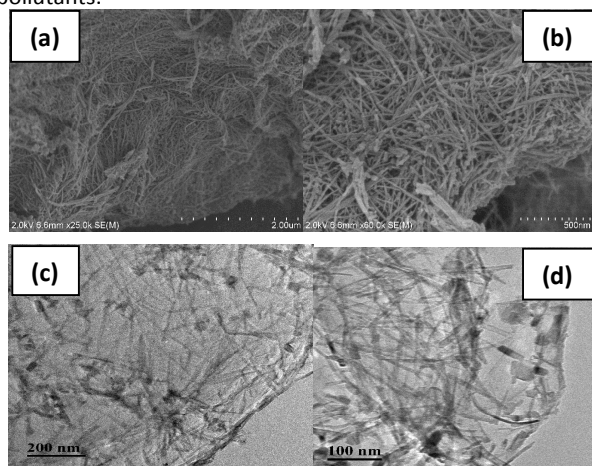


Fig. 4. SEM (a, b) and TEM images (c, d) of Mo-TiO₂NWs/RGO composites.

The light absorption range of the photocatalyst is crucial to its application in solving the environmental problems. The UV-vis DRS of all the as-synthesized samples are exhibited in Fig. 5(a). Compared with TiO₂NWs, which shows little response to visible light, the absorption edge of Mo-TiO₂NWs shifts to the longer wavelength and the response intensity of visible light promotes slightly. This could be explained by the narrower band gap of TiO₂ resulted from Mo-doping⁴³. When incorporated graphene into the matrix of TiO₂NWs, the composites have a broad and intense absorption in visible-light range, which was due to the formation of Ti-O-C bond between TiO₂ and RGO⁴⁴, similar to the instances of carbon-modified TiO₂ composite photocatalysts^{15, 45, 46}. It is noteworthy to notice that compared with TiO₂/RGO composites, Mo-TiO₂NWs/RGO composites show a red shift in the absorption edge and stronger visible light absorption intensity, which can be put down to the formation of doping levels within the band gap of TiO₂NWs because of Mo doping. The effective red shift in the absorption edge and the significantly improved light absorption in visible region are favorable to the photocatalytic activity of Mo-TiO₂NWs/RGO composites. Hence, these features indicate that Mo-

TiO₂NWs/RGO composites could achieve higher photocatalytic activity for photodegradation of MB.

Moreover, by applying Tauc's plot²², the band gap energy (E_g) of all the as-synthesized photocatalysts can be calculated. The curves in Fig. 5(b) exhibit the band gaps of the as-synthesized photocatalysts (obtained by extrapolation) and their values are 3.30, 3.23, 3.13 and 2.98 eV for TiO₂NWs, Mo-TiO₂NWs, TiO₂NWs/RGO and Mo-TiO₂NWs/RGO, respectively. The band gap narrowed from 3.30 to 2.98 eV for TiO₂NWs/RGO, denoting the charge transfer transitions between these three components. Hence, doping with Mo and incorporation of RGO could distinctly change the local electronic structure of TiO₂NWs, thus improving the photocatalytic performance.

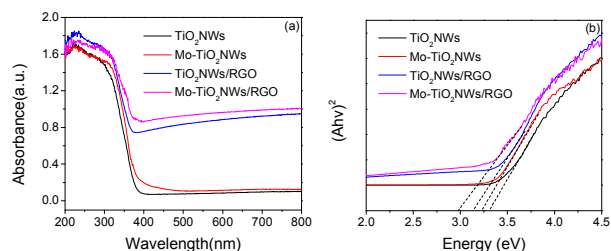


Fig. 5. The UV-vis diffuse reflectance absorption spectra (a) and corresponding Tauc's plot (b) of different photocatalysts.

3.2 Photocatalytic performance and endurance

It is universally known that MB is one of the most representative organic dyes and has been extensively applied in industrial production, which often causes pollution to the environment. Thus, in our study, MB was chosen to be a pollutant model to estimate the photocatalytic activity of different catalysts. The photodegradation tests were performed under visible light irradiation, and the results are shown in Fig. 6. The adsorptive capacity of the photocatalysts was measured by keeping the mixture of MB aqueous solution and photocatalysts in the dark for 1 h to establish adsorption/desorption equilibrium. The results (displayed in Fig. S4(a), ESI[†]) indicate that both the physical mixture of P25+RGO and the photocatalysts without RGO show weak adsorption for MB, while with the incorporation of graphene, the adsorptive capacity for MB is much enhanced, this could be attributed to the π - π conjugation between MB and aromatic regions of RGO^{35, 47}. Such an intensive adsorptivity is favorable for photodegradation of MB on the surface of the photocatalysts³², as illustrated in Fig. 6(a). The self-degradation of MB without photocatalysts is only 5.8%, and the Mo-TiO₂NWs/RGO composites display the highest photocatalytic performance among the tested samples, about 94.1% of the MB was degraded after 120 min under visible light irradiation, while the degradation efficiency is only 33.5%, 41.6%, 59.3% and 83.9% for P25+RGO, TiO₂NWs, Mo-TiO₂NWs and TiO₂NWs/RGO, respectively.

The kinetics of the photodegradation reaction of all the catalysts was fitted to a pseudo-first order equation: $\ln(C_0/C) = kt$, where k is the reaction rate constant (min^{-1}) and t is the

reaction time, as shown in Fig. 6(b). For the blank experiment (no catalysts), the MB decomposes at relatively slow reaction rate with $k=0.0004 \text{ min}^{-1}$. It becomes obvious that the reaction rate constant of MB self-degradation was quite lower than that of the photodegradation of MB with the presence of P25+RGO (0.0025 min^{-1}), TiO_2NWs (0.0031 min^{-1}), Mo-TiO₂NWs (0.0062 min^{-1}), $\text{TiO}_2\text{NWs/RGO}$ (0.0119 min^{-1}) and Mo-TiO₂NWs/RGO (0.0202 min^{-1}). The reaction rate constant of $\text{TiO}_2\text{NWs/RGO}$ for MB degradation was 3.8 times higher than that of TiO_2NWs and the reaction rate constant of Mo-TiO₂NWs/RGO for MB degradation was 3.3 times higher than that of Mo-TiO₂NWs, indicating that the incorporation of RGO significantly strengthened the photocatalytic activity of TiO_2NWs . This is due to the special structure of RGO which can not only strengthen MB adsorptive capacity for gathering reactant to enhance the reaction rate⁴⁸, but also accelerate electron transfer through interfacial interactions to reduce the recombination of photogenerated electron-hole pairs². On the other hand, the reaction rate constants of Mo-TiO₂NWs and Mo-TiO₂NWs/RGO composites for MB degradation were much higher than that of TiO_2NWs and $\text{TiO}_2\text{NWs/RGO}$ composites, respectively, which was because the Mo ions was able to capture the photogenerated carriers to extend the lifetime of carriers or accelerate the separation of carriers⁴³. These results demonstrate that the synergistic effects between Mo doping and RGO significantly improved the visible light photocatalytic activity of TiO_2NWs .

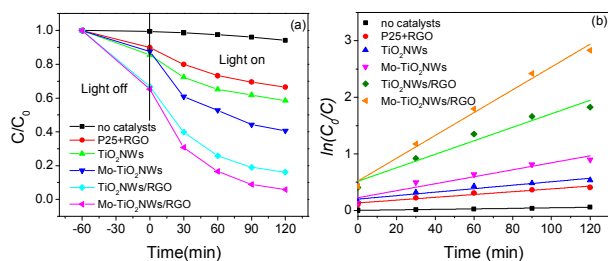


Fig. 6. Photodecomposition curves (a) and the relationship between irradiation time and $\ln(C_0/C)$ (b) of different catalysts for MB, as well as one blank experiment.

Compared to other doped TiO_2 -graphene composites^{37, 48-51}, the Mo-TiO₂NWs/RGO composites show better photocatalytic activity for the degradation of MB (Table S1, ESI[†]). The durability and reusability are the important indicators to evaluate the performance of photocatalysts. The additional recycling experiments exhibited that there was no obvious decrease in photocatalytic degradation efficiency during the five consecutive cycles (Fig. S4(b), ESI[†]), confirming that the Mo-TiO₂NWs/RGO composites were relatively stable during the photocatalytic reactions.

As showed in Fig. 7, first, the excellent adsorption capacity of MB on Mo-TiO₂NWs/RGO composites is not just the simple physical adsorption, but also includes π - π conjugation between MB and RGO due to their aromatic nature. The increased concentration of MB near the catalytic surface is of great advantage to the photodegradation process³². Second,

when light irradiates Mo-TiO₂NWs/RGO composites, electrons are excited from the valence band (VB) to the conduction band (CB), generating excited electrons in the CB and positive holes in the VB. Mo doping results in the narrowing of the band gap, therefore it becomes much easier to separate the photo-generated carriers under the same conditions^{52, 53}. RGO, which acts as both the photo-excited electron acceptor and donor, can succeed in restraining the charge recombination, which will notably promote the photodegradation of MB. Thirdly, the photogenerated electrons react with O_2 molecules which are adsorbed on the surface of TiO_2 to yield the $\cdot\text{O}_2^-$ radical anion and subsequently the $\cdot\text{O}_2^-$ radical anion turns into hydroxide radical ($\cdot\text{OH}$) by protonation and the photogenerated holes interact with $\text{H}_2\text{O/OH}^-$ resulting in the formation of $\cdot\text{OH}$ ⁵³. Then the MB can be decomposed into small molecules through the chain reactions of $\cdot\text{OH}$.

Thus, in this work, the Mo-TiO₂NWs/RGO composites exhibited excellent photocatalytic activity for degradation of MB under visible light irradiation. It is observed that both the incorporation of graphene and Mo doping play important roles in determining the superior photocatalytic activity, and the uniform dispersion of TiO_2NWs on graphene is also crucial for the photocatalytic effect of the composites.

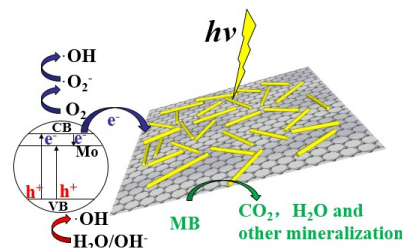


Fig. 7. Schematic illustration of photocatalytic enhancement mechanism of Mo-TiO₂NWs/RGO composites.

4. Conclusions

In this study, a visible-light-stimulated photocatalyst, Mo-TiO₂NWs/RGO composites, has been prepared successfully by alkali hydrothermal route followed by a calcination treatment. Compared with other photocatalysts, the Mo-TiO₂NWs/RGO composites displayed excellent photocatalytic activity in degradation of MB under visible light irradiation. Based on the analysis of the results, the outstanding photocatalytic activity of Mo-TiO₂NWs/RGO composites can be ascribed to the following key factors: (1) morphology modification; (2) Mo doping; and (3) graphene incorporation. All these crucial factors reduce the agglomeration of TiO_2 , strengthen the adsorption of organic compound, narrow the band gap energy, significantly enhance the visible light absorption and promote the separation of photoexcited electron-hole pairs. We believe that this work can enlighten the progress of modified TiO_2 photocatalysts to solve the environmental problems.

Acknowledgements

This research was financially supported by the Fundamental Research Funds for the Central Universities (JUSRP51513) and the Open Project of the International Joint Key Laboratory of Resource Chemistry.

References

1. A. Fujishima and K. Honda, *Nature (London, United Kingdom)*, 1972, **238**, 37-38.
2. J. Hu, H. Li, Q. Wu, Y. Zhao and Q. Jiao, *Chemical Engineering Journal (Amsterdam, Netherlands)*, 2015, **263**, 144-150.
3. Y. Zhang, Z. Zhou, T. Chen, H. Wang and W. Lu, *Journal of environmental sciences*, 2014, **26**, 2114-2122.
4. Z. He, W. Que, J. Chen, X. Yin, Y. He and J. Ren, *ACS Appl Mater Interfaces*, 2012, **4**, 6816-6826.
5. J. Zhang, C. Pan, P. Fang, J. Wei and R. Xiong, *ACS Appl Mater Interfaces*, 2010, **2**, 1173-1176.
6. X.-F. Wu, H.-Y. Song, J.-M. Yoon, Y.-T. Yu and Y.-F. Chen, *Langmuir*, 2009, **25**, 6438-6447.
7. H. Song, S. You, T. Chen and X. Jia, *Journal of Materials Science: Materials in Electronics*, 2015, **26**, 8442-8450.
8. S. Kumar Yadav and P. Jeevanandam, *Ceramics International*, 2015, **41**, 2160-2179.
9. D. Sun, J. Liu, J. Li, Z. Feng, L. He, B. Zhao, T. Wang, R. Li, S. Yin and T. Sato, *Materials Research Bulletin*, 2014, **53**, 163-168.
10. M. A. Ahmed, E. E. El-Katori and Z. H. Gharni, *Journal of Alloys and Compounds*, 2013, **553**, 19-29.
11. S. Umrao, S. Abraham, F. Theil, S. Pandey, V. Ciobota, P. K. Shukla, C. J. Rupp, S. Chakraborty, R. Ahuja, J. Popp, B. Dietzek and A. Srivastava, *RSC Advances*, 2014, **4**, 59890-59901.
12. Q. Huang, S. Tian, D. Zeng, X. Wang, W. Song, Y. Li, W. Xiao and C. Xie, *ACS Catalysis*, 2013, **3**, 1477-1485.
13. Y. Yao, G. Li, S. Ciston, R. M. Lueptow and K. A. Gray, *Environmental Science & Technology*, 2008, **42**, 4952-4957.
14. M. Sun, X. Ma, X. Chen, Y. Sun, X. Cui and Y. Lin, *RSC Advances*, 2014, **4**, 1120-1127.
15. M.-Q. Yang, N. Zhang and Y.-J. Xu, *ACS Applied Materials & Interfaces*, 2013, **5**, 1156-1164.
16. F. Wang and K. Zhang, *Journal of Molecular Catalysis A: Chemical*, 2011, **345**, 101-107.
17. M.-Q. Yang, N. Zhang, M. Pagliaro and Y.-J. Xu, *Chemical Society Reviews*, 2014, **43**, 8240-8254.
18. Y. Zhang, Z.-R. Tang, X. Fu and Y.-J. Xu, *ACS Nano*, 2010, **4**, 7303-7314.
19. W.-S. Wang, D.-H. Wang, W.-G. Qu, L.-Q. Lu and A.-W. Xu, *Journal of Physical Chemistry C*, 2012, **116**, 19893-19901.
20. S. Yu, H. J. Yun, Y. H. Kim and J. Yi, *Applied Catalysis, B: Environmental*, 2014, **144**, 893-899.
21. Y. Liu, *RSC Advances*, 2014, **4**, 36040-36045.
22. T.-D. Nguyen-Phan, V. H. Pham, J. S. Chung, M. Chhowalla, T. Asefa, W.-J. Kim and E. W. Shin, *Applied Catalysis, A: General*, 2014, **473**, 21-30.
23. W. Qian, P. A. Greaney, S. Fowler, S.-K. Chiu, A. M. Goforth and J. Jiao, *ACS Sustainable Chemistry & Engineering*, 2014, **2**, 1802-1810.
24. D. Zhang, Y. Gao, X. Pu, W. Li, C. Su, P. Cai and H. J. Seo, *Science of Advanced Materials*, 2014, **6**, 2632-2639.
25. X. Cao, G. Tian, Y. Chen, J. Zhou, W. Zhou, C. Tian and H. Fu, *Journal of Materials Chemistry A: Materials for Energy and Sustainability*, 2014, **2**, 4366-4374.
26. W. Li, X. Liu and H. Li, *Journal of Materials Chemistry A: Materials for Energy and Sustainability*, 2015, **3**, 15214-15224.
27. T. Zhang, B. Yu, D. Wang and F. Zhou, *Journal of Power Sources*, 2015, **281**, 411-416.
28. J. Li, D. Wang, H. Liu and Z. Zhu, *Materials and Manufacturing Processes*, 2012, **27**, 631-635.
29. K. Bhattacharyya, J. Majeed, K. K. Dey, P. Ayyub, A. K. Tyagi and S. R. Bharadwaj, *J. Phys. Chem. C*, 2014, **118**, 15946-15962.
30. S.-Y. Luo, B.-X. Yan and J. Shen, *Thin Solid Films*, 2012, **522**, 361-365.
31. W. S. Hummers, Jr. and R. E. Offeman, *Journal of the American Chemical Society*, 1958, **80**, 1339.
32. S. D. Perera, R. G. Mariano, K. Vu, N. Nour, O. Seitz, Y. Chabal and K. J. Balkus, *ACS Catalysis*, 2012, **2**, 949-956.
33. M. Zhang, J. Wu, J. Hou and J. Yang, *Science of Advanced Materials*, 2013, **5**, 535-541.
34. H. Li and X. Cui, *International Journal of Hydrogen Energy*, 2014, **39**, 19877-19886.
35. X. Pan, Y. Zhao, S. Liu, C. L. Korzeniewski, S. Wang and Z. Fan, *ACS Applied Materials & Interfaces*, 2012, **4**, 3944-3950.
36. Y. Haldorai, A. Rengaraj, C. H. Kwak, Y. S. Huh and Y.-K. Han, *Synthetic Metals*, 2014, **198**, 10-18.
37. M. Xing, X. Li and J. Zhang, *Scientific reports*, 2014, **4**, 5493.
38. M. Sun, W. Li, S. Sun, J. He, Q. Zhang and Y. Shi, *Materials Research Bulletin*, 2015, **61**, 280-286.
39. W. Wang, C. Lu, Y. Ni and Z. Xu, *Applied Catalysis, B: Environmental*, 2013, **129**, 606-613.
40. Q. Zhai, B. Tang and G. Hu, *Journal of Hazardous Materials*, 2011, **198**, 78-86.
41. P. Dong, Y. Wang, L. Guo, B. Liu, S. Xin, J. Zhang, Y. Shi, W. Zeng and S. Yin, *Nanoscale*, 2012, **4**, 4641-4649.
42. X. Yin, H. Zhang, P. Xu, J. Han, J. Li and M. He, *RSC Advances*, 2013, **3**, 18474-18481.
43. S. Wang, L. N. Bai, H. M. Sun, Q. Jiang and J. S. Lian,

ARTICLE

Journal Name

- Powder Technology*, 2013, **244**, 9-15.
44. H. Zhang, X.-J. Lv, Y.-M. Li, Y. Wang and J.-H. Li, *ACS Nano*, 2010, **4**, 380-386.
45. S. Sakthivel and H. Kisch, *Angewandte Chemie, International Edition*, 2003, **42**, 4908-4911.
46. W. Ren, Z. Ai, F. Jia, L. Zhang, X. Fan and Z. Zou, *Applied Catalysis, B: Environmental*, 2007, **69**, 138-144.
47. Q. Xiang, J. Yu and M. Jaroniec, *Chem Soc Rev*, 2012, **41**, 782-796.
48. C. Liu, L. Zhang, R. Liu, Z. Gao, X. Yang, Z. Tu, F. Yang, Z. Ye, L. Cui, C. Xu and Y. Li, *Journal of Alloys and Compounds*, 2016, **656**, 24-32.
49. N. R. Khalid, E. Ahmed, Z. Hong and M. Ahmad, *Applied Surface Science*, 2012, **263**, 254-259.
50. J.-W. Shi, H.-Y. Ai, J.-W. Chen, H.-J. Cui and M.-L. Fu, *Journal of Colloid and Interface Science*, 2014, **430**, 100-107.
51. Y. Liu, S. Wang, S. Xu and S. Cao, *Materials Research Bulletin*, 2015, **65**, 27-35.
52. L. Gomathi Devi, B. Narasimha Murthy and S. Girish Kumar, *Chemosphere*, 2009, **76**, 1163-1166.
53. Y.-F. Li, D. Xu, J. I. Oh, W. Shen, X. Li and Y. Yu, *ACS Catalysis*, 2012, **2**, 391-398.

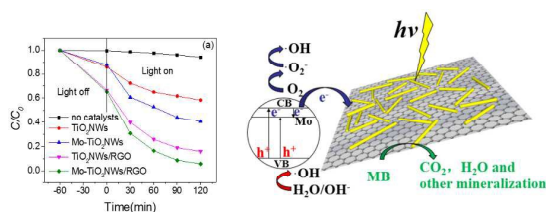
Graphical Abstract

Synthesis of Mo-doped TiO₂ Nanowires/Reduced Graphene Oxide Composites with Enhanced Photodegradation Performance under Visible Light Irradiation

Shanshan Zhu,^a Yuming Dong,^a Xiaofeng Xia,^a Xiang Liu^{*a} and Hexing Li^{*b}

^aThe Laboratory of Food Colloids and Biotechnology, Ministry of Education, School of Chemical and Material Engineering, Jiangnan University, Wuxi 214122, P. R. China. E-mail: liuxiang@jiangnan.edu.cn

^bThe Key Laboratory of the Chinese Ministry of Education in Resource Chemistry, Shanghai Normal University, Shanghai 200234, P. R. China. E-mail: hexing-li@shnu.edu.cn



Mo-doped TiO₂ nanowires/reduced graphene oxide composites with improved visible-light photocatalytic activity were first synthesized, the photocatalytic mechanism was also discussed.